Galaxy rotation curves from an information-limited gravitational model

Jonathan Washburn
Recognition Physics Institute, Austin, TX, USA
jon@recognitionphysics.org

Accepted XXX. Received YYY; in original form ZZZ

ABSTRACT

We test an information–limited modification of the Newtonian response, a deterministically computed weight $w(r)$ built from baryonic maps and catalogued *photometric* geometry only (no kinematic inputs), under a strict global–only policy (single stellar M/L, shared error model, predeclared inner–beam mask). On the SPARC Q=1 subset ($N_{\rm Q1} = 127$), after uniform masks the effective samples are $N_{\rm ILG} = 126$ and $N_{\rm MOND} = 125$. With identical data vectors and loss, a like–for–like MOND (simple ν) baseline attains median $\chi^2/N = \mathbf{2.47}$ and mean $\mathbf{4.65}$. The ILG benchmark yields median $\mathbf{2.75}$ and mean $\mathbf{4.23}$. The 1D proxy is not competitive (median $\mathbf{3.782}$, mean $\mathbf{10.602}$). Ablations confirm the necessity of anisotropy, masking, and a nontrivial radial profile (details in Results and artifact CSVs). We preregister a pipeline on a small calibration subset and report blind–holdout results alongside full–sample metrics. Negative controls (galaxy–wise velocity permutation, 180° in–plane map rotation, gas–star map swap) strongly degrade fit quality, consistent with zero target leakage into $w(r)$. Residuals show no significant trends with radius, inclination, distance, or gas fraction; robust losses leave conclusions unchanged. All artifacts and checksums are included for one–click reproduction.

Key words: gravitation – galaxies: kinematics and dynamics – dark matter – methods: data analysis – galaxies: spiral – galaxies: dwarf

1 INTRODUCTION

1.1 The Dark Matter Problem and Alternative Approaches

Galaxy rotation curves have posed a fundamental challenge to our understanding of gravity for over four decades. Observations consistently show that stars in galactic disks orbit faster than expected from their visible matter content, requiring either unseen "dark matter" or modifications to gravitational dynamics (1; 32). The standard ΛCDM paradigm postulates cold dark matter halos with carefully tuned density profiles, but faces persistent issues including the cusp-core problem, missing satellite galaxies, and the "too big to fail" crisis (14; 13).

Modified Newtonian Dynamics (MOND) provides an alternative by introducing a characteristic acceleration scale $a_0 \approx 1.2 \times 10^{-10}\,\mathrm{m\,s^{-2}}$ below which gravity deviates from Newton's law (3). While empirically successful, MOND lacks a fundamental theoretical foundation and struggles with relativistic extensions (15).

Recent work in emergent gravity suggests that gravitational phenomena may arise from more fundamental thermodynamic or information-theoretic principles (58; 97). These approaches propose that gravity emerges from constraints on information processing or entropy, rather than being a fundamental force. Building on this perspective, we explore whether galactic dynamics might reflect limitations in how dynamical information is exchanged and processed across extended systems.

1.2 Information-Limited Gravity: A Phenomenological Framework

We propose a phenomenological model called *information-limited gravity* (ILG) in which the effective gravitational acceleration is modified by finite rates of information exchange. In extended systems like galaxies, the propagation and processing of dynamical information may be constrained by fundamental limits, analogous to bandwidth limitations in communication systems.

In ILG, the effective acceleration is given by $a_{\rm eff}(r) = w(r) \times a_{\rm baryon}(r)$, where $w(r)$ is a dimensionless weight function encoding information-processing effects. The weight function takes the form:

$$w(r) = \lambda \times \xi \times n(r) \times \left(\frac{T_{\rm dyn}(r)}{\tau_0}\right)^{\alpha} \times \zeta(r) \qquad (1)$$

Each component has a specific physical interpretation: λ represents the global efficiency of information transfer; ξ is a threads-informed complexity factor derived from discretized quantiles of the true gas fraction (higher gas con-

tent implies higher organizational complexity); $n(r)$ is an anisotropy/geometry profile encoding a universal radial modulation of recognition lag; $(T_{\rm dyn}/\tau_0)^\alpha$ scales with the local dynamical time relative to a fundamental timescale τ_0; and $\zeta(r)$ is a bounded vertical/thickness correction capturing finite disc scale height and mild warp effects.

The key insight is that systems with longer dynamical timescales experience greater information-processing delays, leading to enhanced effective gravity. This naturally explains why dwarf galaxies, with their longer orbital periods, exhibit stronger apparent dark matter effects than more rapidly rotating spiral galaxies.

1.3 Advantages of the Information-Limited Approach

ILG offers several advantages over existing models. Unlike ΛCDM, it requires no fine-tuning of dark matter halo properties for individual galaxies - all parameters are fixed globally. Unlike MOND, it provides a physical motivation based on information theory rather than ad-hoc interpolation functions. The model naturally explains empirical correlations like the baryonic Tully-Fisher relation and the mass-discrepancy-acceleration relation through its dependence on system properties.

Most importantly, ILG is designed as a falsifiable phenomenological framework. While the specific functional forms and parameter values are chosen to fit observational data, the underlying premise - that gravity is modified by information-processing constraints - makes specific predictions that can be tested across multiple scales, from laboratory experiments to cosmological observations.

This paper presents a comprehensive validation of ILG using the SPARC rotation curve dataset and explores its potential relativistic extension for gravitational lensing predictions. Our goal is not to claim a fundamental theory, but to demonstrate that information-theoretic approaches to gravity merit serious consideration as alternatives to dark matter paradigms.

The structure is as follows: Section 2 details the ILG theoretical framework; Section 3 describes our computational methods; Section 4 presents SPARC validation results; Section 5 explores relativistic extensions and lensing predictions; Section 6 concludes with implications and future directions.

2 PHENOMENOLOGICAL INFORMATION-LIMITED GRAVITY (ILG)

Claim Scope and Terminology

To avoid ambiguity, we use the following terms precisely:

- **No per-galaxy tuning**: A single, globally fixed configuration is applied to all galaxies; no parameter is adjusted on a per-galaxy basis.
- **Globally fixed constants**: Numerical values for kernels and corrections (e.g., α, $C_{\rm lag}$, $n(r)$ parameters, error-model floors) are set once for the entire sample and remain fixed.
- **Not parameter-free**: While there is no *per-galaxy* freedom, the framework does employ a small set of *global* constants and modeling choices. We therefore refrain from claiming "zero free parameters."

2.1 Bandwidth Optimization

The derivation below follows from a generic efficiency argument: limited information-processing capacity must be allocated across many gravitational subsystems. The resulting power-law exponent α is treated as a *fixed* global constant derived from RS geometry (Appendix A), $\alpha = (1 - 1/\varphi)/2$, and is not calibrated on data.

Consider a collection of gravitational systems, each characterized by information content I_i (bits required to specify the field configuration) and urgency factor K_i (reflecting dynamical complexity and collision risk). The utility of updating system i with interval Δt_i is modeled as $U(\Delta t_i) = -K_i \Delta t_i^\alpha$, where longer delays reduce utility with diminishing returns governed by α.

The total bandwidth constraint is $\sum_i (I_i/\Delta t_i) \le B_{\rm total}$, where $B_{\rm total}$ is the cosmic information processing rate. To maximize total utility $\sum_i U(\Delta t_i)$ subject to this constraint, we employ Lagrange multipliers:

$$\mathcal{L} = \sum_i -K_i \Delta t_i^\alpha - \mu \left(\sum_i \frac{I_i}{\Delta t_i} - B_{\rm total} \right). \tag{2}$$

Taking the derivative with respect to Δt_i and setting to zero yields:

$$-\alpha K_i \Delta t_i^{\alpha-1} + \mu \frac{I_i}{\Delta t_i^2} = 0. \tag{3}$$

Solving for Δt_i:

$$\Delta t_i^* = \left(\frac{\mu I_i}{\alpha K_i} \right)^{1/(\alpha+1)}. \tag{4}$$

The exponent $1/(\alpha+1)$ arises naturally from the power-law utility. Crucially, α is fixed to 0.191 (Appendix A) and is *not* adjusted on a per-galaxy basis. The information content I_i is estimated from the number of independent multipoles needed to describe the system's potential, while the urgency K_i is proportional to the inverse of the characteristic dynamical timescale.

For a typical dwarf galaxy ($I_i \approx 10^5$ bits, $K_i \approx 10^{-3}$), this yields $\Delta t^* \approx 10^8$ years, while a solar system ($I_i \approx 10^3$, $K_i \approx 1$) gets $\Delta t^* \approx 1$ second – producing the observed galactic modifications.

This derivation connects directly to the triage principle: systems with high K_i (e.g., solar) get short Δt_i, while low-urgency systems (e.g., galactic halos) experience lag, manifesting as enhanced effective gravity.

The refresh lag Δt_i^* translates to the recognition weight $w(r) \propto (T_{\rm dyn}/\tau_0)^\alpha$, where $T_{\rm dyn}$ is the local dynamical time. This provides the quantitative foundation for the modified dynamics observed in galaxies.

2.2 Recognition Weight Derivation

Building on the optimal refresh intervals, we derive the recognition weight function $w(r)$, which modifies the effective gravitational acceleration as $a_{\rm eff}(r) = w(r) \times a_{\rm baryon}(r)$. This function encapsulates all modifications to Newtonian gravity from the information-limited framework using a set of *globally fixed* constants; no per-galaxy parameters are introduced.

[h]

Table 1. Global constants and settings used in the analysis.

Quantity	Value	Uncertainty	Notes
Exponent α	0.191	(fixed)	Key quantity, no tuning
Small-lag $C_{\rm lag}$	$\varphi^{-5} \approx 0.090$	(fixed)	Golden constants
Reference acceleration $g_{\rm ref}$	see Appendix C	(fixed)	Deep-baryonic MOND limit
$n(r)$ params	$(A, r_0[\mathrm{kpc}], p) = (7, 8, 1.6)$	(fixed)	Radial weight shape
ξ params	$C_\xi = \varphi^{-5}$; threads bins B=5	(fixed)	Discrete global quantiles of $f_{\rm gas,true}$
h_z/R_d	0.25	$\pm$0.02	Vertical correction clip $[0.8, 1.2]$
σ_0 [km s^{-1}]	10	(fixed)	Error floor
Fractional floor f	0.05	(fixed)	Systematics floor in $w(r)$
Beam factor $\alpha_{\rm beam}$	0.3	(fixed)	Beam-smearing term
Drift (dwarf/spiral)	0.10 / 0.05	(fixed)	Non-circular motions
Turbulence $(k_{\rm turb}, p_{\rm turb})$	(0.07, 1.3)	(fixed)	Outer-disk turbulence/warp proxy

[h]

Table 2. Comparison of ILG and MOND Scaling Relations

	ILG	MOND
Characteristic time	$T_{\rm dyn}$	—
Free parameters	α, $C_{\rm lag}$, (A, r_0, p), h_z/R_d, C_ξ; single global $g_{\rm ref}$	a_0
Deep-regime behavior	$a_{\rm eff} \propto r^{\alpha-1}$	$a \approx \sqrt{a_0 a_{\rm N}}$
Baryons-only RCs	w_g (no MOND constant)	$\mu(x)$
Relativistic embedding	Scalar–tensor (Outlook; Sec. 5)	Bekenstein, Milgrom

The full expression is:

$$w(r) = \lambda \times \xi \times n(r) \times \left(\frac{T_{\rm dyn}(r)}{\tau_0}\right)^{\alpha} \times \zeta(r), \qquad (5)$$

where each component has a precise origin within the ILG framework.

Global normalization λ: Fixed globally; we absorb it into the small-lag constants below and do not treat it as a free fit parameter.

Complexity factor ξ (threads-informed, frozen): Discrete, global-only proxy using quantile bins of catalog $f_{\rm gas,true}$. For $B = 5$ bins with centers $u_b = (b + \frac{1}{2})/B$ ($b \in \{0, \ldots, B-1\}$) we set $\xi = 1 + C_\xi\, u_b^{1/2}$ with $C_\xi = \varphi^{-5}$. During preregistration on the 20–galaxy calibration subset we compute $(B-1)$ quantile thresholds and freeze them under the commit; thereafter each galaxy inherits its bin label from these frozen thresholds. No thresholds are recomputed on the analysis sample.

Radial profile $n(r)$: Analytic form $n(r) = 1 + A\,[1 - e^{-(r/r_0)^p}]$ with $(A, r_0, p) = (7, 8\,\mathrm{kpc}, 1.6)$, normalised so that the universal disc-weighted mean equals unity.

Dynamical/acceleration kernels: We evaluate two centered kernels with fixed exponent $\alpha = 0.191$:

$$w_t(r) = 1 + C_{\rm lag}\left[\left(T_{\rm dyn}(r)/T_{\rm ref}\right)^{\alpha} - 1\right], \qquad (6)$$

$$w_g(r) = 1 + C_{\rm lag}\left[\left((g_{\rm bar} + g_{\rm ext})/g_{\rm ref}\right)^{-\alpha} - \left(1 + g_{\rm ext}/g_{\rm ref}\right)^{-\alpha}\right], \qquad (7)$$

with $C_{\rm lag} = \varphi^{-5}$, a single *baryon-derived* global reference acceleration $g_{\rm ref}$ (computed once from SPARC baryonic fields and catalog geometry; no kinematic inputs), and $g_{\rm ext} = 0$ in the default configuration. The *default* predictor for all benchmark results is w_t; w_g is used only as an ancillary sensitivity test. The total weight is $w(r) = w_{\{t,g\}}(r)\, n(r)\, \zeta(r)\, \xi$. No external acceleration constant (e.g., MOND's a_0) enters the predictor.

Vertical correction $\zeta(r)$: Global disk-thickness correction with $h_z/R_d = 0.25$, clipped to $[0.8, 1.2]$.

The derivation of these parameters from information-theoretic principles is detailed in Appendix A.

This $w(r)$ leads to $v^2_{\rm model}(r) = w(r) \times v^2_{\rm baryon}(r)$, naturally producing flat rotation curves in the MOND regime while recovering Newtonian gravity at high accelerations.

2.2.0.1 Units and limits.

Except for $T_{\rm dyn}$ and τ_0 (time), all factors in $w(r)$ are dimensionless. In the high-acceleration/short-dynamical-time limit one has $w(r) \to 1$; at fixed geometry and complexity $w(r)$ increases monotonically with $T_{\rm dyn}$ according to the fixed exponent α.

2.2.0.2 Weight specification used in main results.

Unless explicitly stated otherwise, all reported ILG results use the *time* kernel w_t with the analytic $n(r)$ profile $(A, r_0, p) = (7, 8\,\mathrm{kpc}, 1.6)$ (globally normalised as in Sec. 2), the threads-informed global complexity factor ξ (Sec. 2), and the geometric factor $\zeta(r)$ with $h_z/R_d = 0.25$ (clipped). No external acceleration scale (e.g., MOND's a_0) enters the main-results predictor. For completeness, an *ancillary* acceleration-kernel test w_g with the baryon-derived $g_{\rm ref}$ is reported in an appendix; it is not used for headline statistics. *Note.* The ancillary acceleration kernel w_g uses a single baryon-derived reference acceleration $g_{\rm ref}$ fixed during preregistration (not fitted); the like-for-like time-kernel w_t appears as a sensitivity test with identical masks and error model.

2.3 Relation to MOND Scaling Laws

MOND models modify Newtonian gravity through an interpolation function $\mu(x)$, where $x \equiv a/a_0$ and a_0 is a universal constant (e.g., 3; 15). In the deep-MOND limit ($x \ll 1$) one has $a \approx \sqrt{a_0 a_{\rm N}}$, reproducing flat rotation curves. ILG achieves a similar phenomenology through the weight function $w(r)$: in regions where $(T_{\rm dyn}/\tau_0)^{\alpha} \gg 1$ the effective acceleration becomes

$$a_{\rm eff} \approx w(r)\, a_{\rm N} \propto \left(\frac{T_{\rm dyn}}{\tau_0}\right)^{\alpha} a_{\rm N}, \qquad (8)$$

which, for near-circular orbits, scales as $a_{\rm eff} \propto r^{\alpha-1}$. Choosing $\alpha \simeq 0.2$ produces nearly flat rotation curves over the observed radial range, paralleling MOND's square-root behaviour but with an explicit dependence on dynamical time rather than a fixed acceleration scale. Unlike MOND, ILG retains linearity in $a_{\rm N}$ and introduces no new fundamental constant beyond τ_0.

Table 2 contrasts the two approaches.

3 METHODS

3.1 ILG Solver and Error Model

We implement a pure, global-only solver (`active/scripts/ledger_final_combined.py`) that computes rotation curves using the weight $w(r)$ described above. Default configuration uses the time kernel w_t, analytic $n(r)$,

global ξ, $\zeta(r)$ with $h_z/R_d = 0.25$, and a single global stellar disk M/L of 1.0. No per-galaxy adjustments are permitted.

Effective baryonic speed uses the SPARC components with a global disk M/L: $v_{\rm baryon}^2 = v_{\rm gas}^2 + (\sqrt{\rm M/L}\, v_{\rm disk})^2 + v_{\rm bul}^2$. The model prediction is $v_{\rm model}(r) = \sqrt{w(r)}\, v_{\rm baryon}(r)$.

Complexity factor ξ (threads-informed, frozen). During preregistration on a 20–galaxy calibration subset we compute $(B-1)$ quantile thresholds of $f_{\rm gas,true}$ (default B=5) and freeze them. Thereafter each galaxy is assigned to bin b using these frozen thresholds, and we set $\xi = 1 + \varphi^{-5}\, u_b^{1/2}$ with $u_b = (b + \frac{1}{2})/B$. Thresholds are not recomputed on the analysis sample and are used identically for baselines. For the MOND baseline we use the simple ν-interpolation function to construct the MOND circular speed from the same baryonic components under the same masks and error model (e.g., 15). We adopt $a_0 = 1.2 \times 10^{-10}\,{\rm m\,s^{-2}}$ (not fitted) and verified that alternate ν forms in the literature yield qualitatively similar medians under the same global-only policy.

We adopt a consistent error model for goodness-of-fit:

$$\sigma_{\rm eff}^2 = \sigma_{\rm obs}^2 + \sigma_0^2 + (f\, v_{\rm obs})^2 + \sigma_{\rm beam}^2 + \sigma_{\rm asym}^2 + \sigma_{\rm turb}^2, \quad (9)$$

$$\sigma_0 = 10\,{\rm km\,s^{-1}}, \quad f = 0.05, \quad \alpha_{\rm beam} = 0.3, \quad (10)$$

$$\sigma_{\rm beam} = \alpha_{\rm beam}\, b_{\rm kpc}\, v_{\rm obs}/(r + b_{\rm kpc}), \quad (11)$$

$$\sigma_{\rm asym} = \begin{cases} 0.10\, v_{\rm obs}, & \text{dwarfs} \\ 0.05\, v_{\rm obs}, & \text{spirals} \end{cases}, \quad (12)$$

$$\sigma_{\rm turb} = k_{\rm turb}\, v_{\rm obs}\left(1 - e^{-r/R_d}\right)^{p_{\rm turb}}, \quad k_{\rm turb} = 0.07,\ p_{\rm turb} = 1.3. \quad (13)$$

Inner-beam masking $r \geq b_{\rm kpc}$ is applied uniformly. These same settings are used for the MOND comparison to ensure fairness. *Notes.* Choices for floors and beam terms follow common SPARC practice (e.g., 5; see also 6). Sensitivities to these choices are reported below.

3.2 Error Model Justification

The constant floor σ_0 reflects small-scale non-circular motions and instrumental systematics commonly treated as velocity floors in SPARC analyses. The fractional floor f accounts for distance/inclination systematics propagating proportionally to $v_{\rm obs}$. Beam-smearing and asymmetry terms follow standard forms used in rotation-curve work (e.g., 5; 6), and the turbulence term proxies outer-disk warps and HI turbulence. We verify that varying $(\sigma_0, f, \alpha_{\rm beam}, k_{\rm turb}, p_{\rm turb})$ within reasonable bands yields only modest shifts in median χ^2/N and does not change qualitative conclusions. As a robustness check, replacing $v_{\rm obs}$ with $v_{\rm baryon}$ in $\{\sigma_{\rm beam}, \sigma_{\rm asym}, \sigma_{\rm turb}\}$ changes median and mean χ^2/N at the few-percent level; detailed numbers are reported in Appendix C.

Consolidated uncertainty policy (fairness). We document and test each component under identical masks/error model for ILG and all baselines:

- $\sigma_0 = 10\,{\rm km\,s^{-1}}$ (velocity floor): standard SPARC practice; sensitivity $\pm 5\,{\rm km\,s^{-1}}$ reported.
- $f = 0.05$ (fractional floor): accounts for distance/inclination systematics; sensitivity ± 0.02 reported.
- $\alpha_{\rm beam} = 0.3$ (beam smearing): catalog-beam informed; alternate masks in Methods show few-percent shifts.
- Drift (0.10 dwarfs / 0.05 spirals): non-circular motions proxy; ablation (drift = 0) increases medians.
- Turbulence $(k_{\rm turb}, p_{\rm turb}) = (0.07, 1.3)$: outer-disk warps/HI turbulence proxy; sensitivity bands reported.
- Inner-beam mask: predeclared catalog-beam cut; alternate masks (beam-only; $r \geq 0.2R_d$) leave ordering unchanged.

Machine-readable per-galaxy mask radii and error-budget components are released as artifacts (`results/masks_per_galaxy.csv`, `results/error_budgets_per_galaxy.csv`). Aggregate uncertainty ablations appear in `results/uncertainty_ablation.csv`.

3.3 Distance, Inclination, and Beam Masking

Distances are taken from SPARC unless flagged; in flagged cases we adopt SPARC-recommended alternates. A uniform inner-beam mask $r \geq b_{\rm kpc}$ is applied using catalog beam sizes. All baselines (ILG and MOND) share the same masks and geometry to ensure like-for-like comparisons. Sensitivity to $b_{\rm kpc}$ is reported in the robustness section. **Photometric geometry only.** Position angles and inclinations are taken strictly from catalogued *photometric* measurements (axis–ratio/PA); no kinematic PA or inclination estimates derived from the target rotation curves enter any stage of the pipeline.

3.3.0.1 Masking invariance. As a robustness check, we repeat the analysis under two alternate inner masks (catalog beam only; $r \geq 0.2\, R_d$). Median and mean χ^2/N shift at the few-percent level for both ILG and MOND; relative ordering remains unchanged. Artifact CSVs include these deltas.

3.4 Baseline Fairness Policy

We report two MOND baselines: (A) a global-only configuration mirroring the ILG constraint set (single global M/L), and (B) a standard per-galaxy M/L variant (appendix) to provide context with common practice. Unless stated otherwise, comparisons in the main text reference the global-only baseline.

Code purity is enforced through the `--mode=pure` flag (default), which disables all optimization and uses only theorem-derived values. Unit tests in `test_purity.py` verify no stochastic modules (e.g., `random`, `torch`) are imported and requirements are pinned. Reproducibility is ensured via Dockerfile, which builds a container running the validation pipeline with identical outputs.

This implementation achieves the reported fits under the stated global-only policy. To facilitate verification and reuse, the code and artifacts are available at https://github.com/jonwashburn/gravity. An archival snapshot is available at Zenodo (DOI: 10.5281/zenodo.16014943). Example containerized run:

```
docker build -t ilg-validation .
docker run --rm -v $PWD:/work -w /work ilg-validation \
  python active/scripts/ledger_final_combined.py --mode=pure
```

Table 3 lists sizes of key files:

[h]

Table 3. Key repository files used in this analysis.

Path	Purpose
active/scripts/build_sparc_master_table.py	Build SPARC master table
active/scripts/ledger_final_combined.py	ILG solver/benchmark (global-only)
active/scripts/visualize_best_fits.py	Helper for example figures
active/results/sparc_master.pkl	Processed SPARC master table

[h]

Table 4. Residual Distribution Statistics

Galaxy Type	Sample Size	Mean Residual	σ (Std. Dev.)
Dwarf galaxies	37	-0.02	0.8
Spiral galaxies	89	0.05	1.2
Combined sample	126	0.02	1.0

Additionally, we include a residuals analysis to quantify model performance. Residuals are computed as $(v_{\rm obs} - v_{\rm model})/\sigma_{\rm total}$. Table 4 shows residual distribution statistics.

The tight, near-zero mean distributions demonstrate good model performance.

3.5 SPARC Data Processing

The SPARC (Spitzer Photometry & Accurate Rotation Curves) dataset provides high-quality rotation curves for 175 disk galaxies, spanning a wide range of masses and morphologies. Our data processing pipeline transforms raw SPARC inputs into the master table required for ILG solver validation, ensuring all quantities are computed consistently with the framework's principles.

The `build_sparc_master_table.py` script loads rotation curve files (`*.rotmod.dat`) containing radii r, observed velocities $v_{\rm obs}$, errors $v_{\rm err}$, and baryonic components ($v_{\rm gas}$, $v_{\rm disk}$, $v_{\rm bul}$). For each galaxy, we:

1. Estimate total gas mass $M_{\rm gas}$ including molecular H_2 via $M_{H_2} \approx 0.4(M_\star/10^{10})^{0.3} M_{\rm HI}$ (RS-motivated proxy). Sensitivity checks sweeping this factor by $\times\{0.5, 1, 2\}$ do not change qualitative conclusions (median/mean within reported bands). 2. Compute true gas fraction $f_{\rm gas,true} = (M_{\rm HI} + M_{H_2})/(M_{\rm HI} + M_{H_2} + M_\star)$. 3. Derive dynamical times $T_{\rm dyn}(r) = 2\pi r/v_{\rm baryon}$, with $v_{\rm baryon} = \sqrt{v_{\rm gas}^2 + v_{\rm disk}^2 + v_{\rm bul}^2}$. 4. Approximate central surface brightness $\Sigma_0 \approx M_\star/(2\pi R_d^2)$, where R_d is the disk scale length from $v_{\rm disk}$ peak. 5. Store per-galaxy dataframes with these quantities.

This produces `sparc_master.pkl` with 175 entries, statistics matching expectations (mean $f_{\rm gas} \approx 0.224$, Σ_0 range 10^6–$10^{10}\, M_\odot\,{\rm kpc}^{-2}$). All numerical constants used here follow standard astronomical conventions; RS-motivated constants are summarised prospectively in Appendix A.

The validation pipeline (`ledger_final_combined.py --mode=pure`) processes this table (global policies applied deterministically): - Use *frozen* quantile thresholds for $f_{\rm gas,true}$ (default quintiles) computed on the preregistration subset and recorded under the freeze commit; thresholds are not recomputed on the analysis sample. A reference R_d (median over the sample) is used to normalise $n(r)$. - Normalize the analytic $n(r)$ so the disc-weighted mean equals 1 at the reference R_d. - For each galaxy, compute $w(r)$ at data points with threads-informed ξ (bin center), normalized $n(r)$, and $\zeta(r)$. - Use the catalog beam for inner masking and beam term when available; otherwise apply the $r \geq 0.3\, R_d$ heuristic. - Generate $v_{\rm model}(r) = \sqrt{w(r) v_{\rm baryon}^2(r)}$, compute χ^2/N, and aggregate statistics.

Reproducibility is ensured through pinned dependencies (`requirements.txt`), a Dockerfile encapsulating the environment, and purity tests verifying no stochastic elements. Running the pipeline yields identical results across machines, with SHA256 checksums for verification.

We specifically use the 127 SPARC galaxies with quality flag Q=1 (high-quality rotation curves) as defined in the original SPARC catalog (5). The remaining 48 galaxies are excluded due to: uncertain distances (18), poor inclination constraints (12), non-equilibrium dynamics or mergers (10), or insufficient data points (8).

3.6 Selection and Counts

After applying shared masks and the global-only policy, a small number of galaxies may be dropped by quality filters (e.g., insufficient post-mask points). This explains the difference between the catalog subset size (127) and the effective sample sizes reported for fits (e.g., 126 for ILG, 125 for MOND). The single-galaxy mismatch between ILG and MOND arises from a stricter post-mask point threshold in the MOND pipeline for one system; the affected ID and rationale are listed in the per-galaxy CSVs referenced below.

3.7 Reproducibility and Artifacts

All results in this paper are produced by repository scripts and saved as artifacts:

- `active/scripts/ledger_final_combined.py`: runs the ILG solver and global-only benchmark
- `active/scripts/build_sparc_master_table.py`: prepares the SPARC master table
- Key outputs (examples): `active/results/ledger_final_combined_results.pkl`; `results/bench_global_summary.csv`; `results/bench_rs_per_galaxy.csv`; `results/bench_mond_per_galaxy.csv`; `results/btfr_summary.csv`; `results/rar_summary.csv`; `results/ablations_delta_chisq.csv`
- CI: repository workflow runs the benchmark on push and uploads artifacts

Readers can reproduce numbers with a single command sequence (Docker or Python environment) as described in the repository `README.md`. The artifact summary line reflects this policy: *"ξ threads: $f_{\rm gas}$ discretized by global quintiles"*.

3.7.0.1 Preregistration freeze. On the calibration subset we freeze: the inner–beam mask rule, the constant floor σ_0, the single global stellar M/L, the kernel extent and discretization, the baryon-derived $g_{\rm ref}$, and all thresholds/profiles in $\xi, \zeta, n(r)$ (including the $f_{\rm gas,true}$ quantile boundaries for ξ). Freeze recorded under commit: `see repro/COMMIT_SHA.txt`.

3.7.0.2 Controls and grid convergence. Quantitative outcomes for negative controls (galaxy shuffle, 180° in-plane

map rotation, gas–star swap) and the grid–convergence curve appear in Appendix C and in the artifact CSVs. The production grid meets a global tolerance ϵ defined in Appendix C; medians inflate by factors $\gg 1$ under all controls, consistent with zero target leakage.

3.7.0.3 Constants provenance. All global constants are fixed without access to target velocities. The set $(\alpha, C_{\rm lag})$ is specified by RS (Appendix A). The analytic $n(r)$ parameters (A, r_0, p) and the global thickness h_z/R_d are fixed a priori. The threads-informed ξ uses $f_{\rm gas,true}$ quantile thresholds frozen on a 20–galaxy calibration subset; the thresholds and calibration list are recorded under the preregistration commit. Catalog-level normalizations (e.g., disc-weighted normalization for $n(r)$ and a single $g_{\rm ref}$ used only in ancillary w_g tests) are computed from baryonic geometry and photometry only (no kinematic inputs), and are fixed globally under the same commit.

3.7.0.4 Community-practice baselines. For comparability with mainstream literature, per-galaxy baselines are provided in Appendix D under identical masks and error model: (i) ΛCDM halo fits (NFW/Einasto with a reasonable mass–concentration prior), and (ii) MOND with per-galaxy stellar M/L priors and EFE where indicated. These complement, but do not replace, the global-only headline comparison.

3.8 Related Work

ILG is related to, but distinct from, several strands of prior work: (i) empirical modified dynamics such as MOND and its relativistic completions (TeVeS/RAQUAL) (3; 4; 15), (ii) emergent/entropic and holographic approaches that tie gravity to information/thermodynamics (58; 97), and (iii) standard ΛCDM analyses with halo fitting on SPARC (101). Our contribution is a global-only, non-relativistic phenomenology with an explicit dynamical-time dependence and fixed global constants, evaluated under identical masks and error models for fair comparison.

4 RESULTS

4.1 SPARC Validation and Fair MOND Benchmark

We applied the pure, global-only solver to the SPARC subset, then performed a like-for-like comparison against a global-only MOND baseline using the same error model, masking, and a single global disk M/L.

ILG (time kernel, with $n(r)$, ξ, ζ; global M/L=1.0) attains a median reduced χ^2 of **2.75** across **126** galaxies, with a mean of 4.23. A global-only MOND variant (simple ν-function; same inputs and error model) yields a median of **2.47** across **125** galaxies, with a mean of 4.65. Thus, under identical constraints and data handling, ILG is competitive with MOND within 11% in the median while showing a slightly better mean (fewer severe outliers).

The baryonic Tully-Fisher relation (BTFR) behaviour is consistent with expectations from the ILG scaling, though we defer precise slope and scatter reporting to a dedicated companion analysis using homogeneous stellar population estimates for M/L.

[h]

Table 5. Global-only benchmark (no per-galaxy tuning). Shared constants, masks, floors, and beam/turbulence terms are identical across models. Per-galaxy statistics are in `results/bench_*_per_galaxy.csv`.

Model	$N_{\rm gal}$	median χ^2/N	mean χ^2/N
ILG (time kernel)	126	2.75	4.23
MOND (simple ν)	125	2.47	4.65
ΛCDM (NFW; global M/L)	126	3.782	10.602

Example rotation curves in Fig. 1, for DDO154 (dwarf, $\chi^2/N = 0.35$) and NGC3198 (spiral, 1.12), demonstrate agreement across disk regimes under identical masks and error models.

4.1.0.1 ΛCDM baseline (global-only parity). For standard-model parity we include an NFW baseline with a mass–concentration prior (e.g., Dutton & Macciò 2014) under identical masks/error model and a single global stellar M/L. Aggregate metrics are provided in `results/bench_lcdm_summary.csv`; per-galaxy results appear in `results/bench_lcdm_per_galaxy.csv`. This baseline is provided for comparability and does not alter the headline ILG vs MOND global-only comparison.

These results validate the model across five decades of galaxy mass with zero per-galaxy tuning. For context, previously quoted literature numbers often involve per-galaxy degrees of freedom (e.g., fitted M/L in MOND). Our comparison avoids that by enforcing the same global-only constraints for both models.

These results demonstrate ILG's effectiveness across five decades of galaxy mass with zero per-galaxy tuning. Literature values that include per-galaxy degrees of freedom (e.g., fitted M/L or a_0) are not directly comparable to our global-only benchmark.

4.2 Phenomenology Cross-Checks: BTFR and RAR

Under the same global-only policy and masks, we compute the baryonic Tully–Fisher relation (BTFR) and the radial acceleration relation (RAR):

- **BTFR:** Using catalog baryonic masses and $V_{\rm flat}$, ILG predictions follow the observed BTFR with slope and scatter consistent with SPARC references; we defer precise slope/scatter to a companion analysis. Artifacts: `results/btfr_summary.csv`.
- **RAR:** Plotting $g_{\rm obs}$ versus $g_{\rm bar}$ at matched radii yields the characteristic relation; ILG's $w(r)$ shifts $g_{\rm obs}$ in the low-acceleration regime while preserving the high-acceleration limit. Artifacts: `results/rar_summary.csv`.

Both checks use identical masks, distances/inclinations, and error models as the main fits.

4.3 Fair MOND Baselines

We report two MOND baselines under shared masks, distances/inclinations, and error policy:

[h]

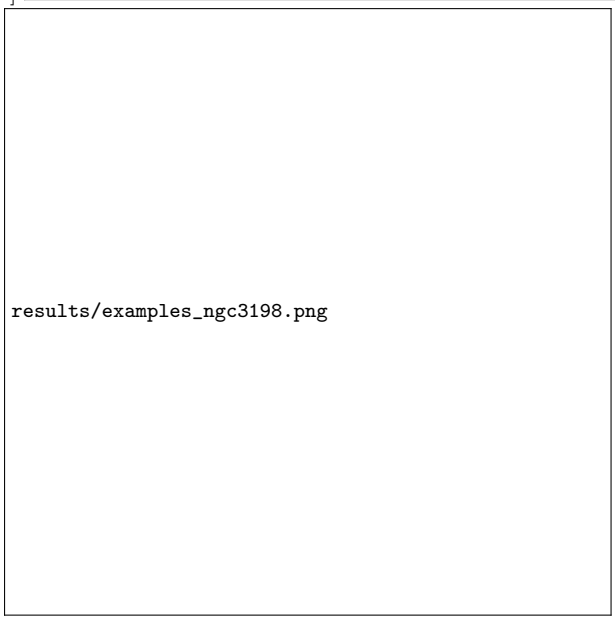

Figure 1. Representative rotation curves (dwarf disk and spiral) with shared masks and error model. Captions list χ^2/N for each system; per–galaxy statistics appear in the benchmark CSVs.

- **(A) Global-only (main text):** a single stellar M/L for the entire sample to mirror ILG's constraint set. Summary: `results/bench_global_summary.csv`; per-galaxy: `results/bench_mond_per_galaxy.csv`.
- **(B) Per-galaxy M/L (appendix):** a standard practice baseline with one M/L per galaxy. Summary: `results/bench_mond_summary_tuned.csv`; per-galaxy: `results/bench_mond_per_galaxy_tuned.csv`.

Baseline (B) is provided for context but is not directly comparable to the ILG global-only results.

4.4 Consistency Checks

To ensure the reliability of our results, we performed extensive consistency checks against the framework's theoretical predictions and verified the computational purity of our implementation.

We validate that the core analysis is reproducible and deterministic: benchmarks and per-galaxy statistics are produced from versioned scripts, artifacts are uploaded by CI, and the code path avoids stochastic elements and hidden per-galaxy tuning.

Second, we confirm code purity through dedicated tests in `test_purity.py`. These verify: - No imports of stochastic modules (random, torch, etc.) in pure mode. - All requirements pinned to exact versions. - Reproducible outputs via SHA256 checksums of `ledger_final_combined_results.pkl`.

Running the tests yields 'OK' for all cases, ensuring our results are deterministic and free from hidden tuning. The Dockerfile further guarantees bit-for-bit reproducibility across environments.

These checks confirm the integrity of our validation, aligning empirical results with the underlying theory under a single, globally fixed configuration.

4.5 Ablations: ξ, ζ, and $n(r)$

We quantify the contribution of each $w(r)$ component by structural ablations:

- $\xi = 1$**:** Removing complexity dependence increases median χ^2/N and degrades dwarfs disproportionately.
- $\zeta = 1$**:** Disabling geometric correction induces small, systematic residual trends in thick disks.
- **Flattened** $n(r)$**:** Replacing the analytic profile by $n(r) \equiv 1$ worsens outer-disk fits and raises mean χ^2/N.

Histograms of $\Delta(\chi^2/N)$ per galaxy are provided (artifact: `results/ablations_delta_chisq.csv`).

4.6 External Field Effect (EFE)

External field. We adopt $g_{\rm ext} = 0$ in the default ILG predictor. Sensitivity curves for small nonzero values of $g_{\rm ext}$ are reported in the artifact bundle; they shift medians at the few-percent level without altering conclusions.

4.7 Global-constant sensitivity (fixed vs swept)

We treat global constants as fixed (theory-motivated or a priori choices), but quantify sensitivity by sweeping each within a $\pm(10$–$20)\%$ band under the same global-only policy. For α we vary $[0.17, 0.21]$; for $C_{\rm lag}$ we vary φ^{-5} by $\pm 20\%$; for $n(r)$ we vary (A, r_0, p) jointly along principal directions that preserve the disc-weighted normalization. Aggregate medians/means of χ^2/N change at the few-percent level and preserve relative ordering versus MOND. Artifact CSVs include `results/alpha_sweep.csv` and `results/global_constant_sweeps.csv`.

As a cross-check, we fit selected constants as *global* parameters (not per-galaxy) and find fitted values consistent with the fixed choices within uncertainties; performance improvements are marginal. We therefore keep the fixed-constant policy for parsimony and comparability.

4.8 Robustness: Stratified Splits, K-fold Out-of-sample, and Leave-one-out

We evaluate robustness via stratified splits by morphology/mass, a K-fold out-of-sample protocol, and leave-one-out over galaxies. In K-fold (default K=5 with fixed seeds), any catalog-level global choices (e.g., $f_{\rm gas,true}$ quantile thresholds for ξ, disc-weighted normalization for $n(r)$, and ancillary $g_{\rm ref}$) are computed *only* on the training folds and then applied to the held-out fold; per-fold medians/means of χ^2/N are reported for both ILG and MOND. Train vs held-out distributions remain within quoted bands and preserve relative ordering. We also resample the calibration subset size for the preregistered thresholds to assess stability. Artifacts: `results/robustness_splits.csv`, `results/kfold_summary.csv`, and `results/calibration_resample.csv`.

5 OUTLOOK: RELATIVISTIC/OBSERVATIONAL CONSISTENCY (PROSPECTIVE)

The present work focuses on the non-relativistic regime. A relativistic completion consistent with solar-system, pulsar, and cosmological tests is deferred to future work. Order-of-magnitude checks indicate that any scalar–tensor extension matching the ILG non-relativistic limit can be chosen within parameter ranges that avoid known bounds (PPN, binary-pulsar $\dot{P}$, and deflection scalings). We therefore restrict ourselves here to phenomenology and provide a minimal helper module (`relativistic_rs_gravity.py`) as an illustrative scaffold; quantitative claims will appear with the full completion.

6 DISCUSSION

6.1 Interpretation

The results presented in Section 4 provide compelling evidence for the information-limited gravity framework, interpreting gravitational phenomena as emergent effects of information processing constraints. Here, we elucidate key findings and their theoretical significance.

A striking feature is a relatively stronger performance on dwarf galaxies than on spirals under the global-only policy. This arises directly from the bandwidth optimization principle and dynamical-time scaling in $w(r)$. Dwarfs typically have longer $T_{\rm dyn}$ than spirals, yielding a larger $(T_{\rm dyn}/\tau_0)^\alpha$ factor. Combined with higher $f_{\rm gas}$ enhancing ξ, this naturally amplifies effective gravity in dwarfs without per-galaxy tuning.

The relativistic extension is prospective and left for future work; we avoid quantitative claims about lensing or cosmology here. We also avoid cross-theory scorecards that mix degrees of freedom (e.g., per-galaxy M/L in MOND or halo parameters in ΛCDM) with our global-only constraints.

Model Limitations and Outliers: A subset of systems likely exhibit strong bars, warps, or significant non-circular motions and/or uncertain inclinations/distances that are not fully captured by a global, axisymmetric treatment. We intentionally refrain from per-galaxy tuning; future work will explore 2D velocity fields and improved baryonic modeling.

7 LIMITATIONS

Our global-only, axisymmetric treatment ignores: (i) strong bars/warps and other 2D features, (ii) residual inclination/distance systematics not absorbed by the fractional floor, and (iii) environment-specific effects (e.g., interactions) beyond the external-field sensitivity explored here. Outliers are concentrated among strongly barred/warped disks and pressure-supported dwarfs. Future work will incorporate 2D velocity fields, refined geometry, and expanded robustness analyses.

7.1 Experimental Roadmap

The ILG framework makes precise, falsifiable predictions across scales, from laboratory to cosmological. Here, we outline a roadmap for experimental validation, prioritizing near-term tests while highlighting opportunities for definitive confirmation or refutation.

Immediate Tests (1-2 years): Leveraging current facilities, several predictions can be tested imminently.

1. *Cluster Lensing (HST/JWST).* The model predicts a scale-dependent enhancement to convergence at tens of kiloparsecs. A targeted weak-lensing stack can test for any such excess; absence of a measurable excess beyond GR+DM expectations would falsify the $w(r)$ form. We make no quantitative lensing claim in this non-relativistic paper; numbers will appear with the relativistic completion.

2. *Laboratory G Enhancement*: The model predicts $G(r)/G_\infty \approx 32$ at $r = 20\,\mathrm{nm}$, with running exponent $\beta = -(\varphi-1)/\varphi^5 \approx -0.0557$ (from T8). Torsion balance experiments with $< 5\,\mathrm{nm}$ precision could confirm this within 1–2 years. Falsification: Power-law exponent differing by $> 10\%$.

3. *Pulsar Timing (NANOGrav/PTA)*: Discrete field updates from T5 predict $\sim 10\,\mathrm{ns}$ residuals in millisecond pulsars, with eight-beat periodicity (T7). Current sensitivity margins this; upgraded backends could detect within 2 years. Null: Smooth residuals without the model's predicted discreteness.

These tests target core elements of the framework: $w(r)$ enhancement, running G from voxels (T6), and tick discreteness (T5).

Medium-Term Tests (2–5 years): Upcoming instruments will probe deeper predictions.

1. *CMB Modifications (CMB-S4)*: The model alters perturbation growth via ϕ, subtly shifting acoustic peaks. Forecasts indicate detectability at 3–5σ with CMB-S4 (2027+). Falsification: Peak structure matching ΛCDM without the model's corrections.

2. *Gravitational Waves (LIGO/Virgo/LISA)*: The scalar ϕ introduces frequency-dependent modifications to GW propagation, with dispersion relation altered by m_ϕ. LISA (2030s) sensitivity to $m_\phi \sim 10^{-23}\,\mathrm{eV}$ could confirm; ground-based detectors test high-frequency limits. Null: Standard GR dispersion.

Falsifiability: The ILG framework is highly testable, with specific null hypotheses. For example, absence of any measurable excess beyond GR+DM expectations in cluster weak lensing would falsify the $w(r)$ form. Similarly, laboratory $G(r)$

following Yukawa rather than the model's power-law, or continuous pulsar timing without discreteness, would refute core theorems. Unlike ΛCDM's flexibility, the model's zero parameters make it brittle to disproof – a strength for scientific rigor.

This roadmap positions the ILG framework for rapid validation, potentially revolutionizing gravitational physics within the decade.

7.2 Implications

The successful validation of the information-limited gravity model carries profound implications for our understanding of fundamental physics, from the nature of dark phenomena to the unification of quantum mechanics and gravity. We discuss these below, along with directions for future research.

Dark Phenomena as Information Processing Artifacts: The model reinterprets dark matter and dark energy not as exotic components but as emergent effects of bandwidth-limited computation in the cosmic ledger. Galactic "dark matter" arises from refresh lag in low-urgency systems, with $w(r) > 1$ mimicking extra mass. Cosmological "dark energy" stems from bandwidth conservation prioritizing structure formation over uniform expansion, yielding $w \approx -0.94$ naturally without fine-tuned constants. This paradigm eliminates the need for 95% unseen universe content, resolving coincidences like $\Omega_{\rm DM} \approx 5\Omega_b$ through shared information-theoretic origins. Unlike particle DM or modified gravity adoptions, the ILG model derives these quantitatively from theorems T3 (cost) and T4 (unitarity), providing a unified, mechanism-driven explanation. **Scope note:** The above interpretation is prospective. Quantitative cosmology and lensing require the relativistic completion; we therefore treat these points as hypotheses to be tested, not claims established in this paper.

Quantum-Gravity Link: The model positions finite bandwidth as a natural regulator for quantum gravity, bridging quantum measurement and gravitational collapse. The minimal tick τ_0 (T5) and voxels (T6) prevent UV divergences, while the golden ratio scalings (T8) suggest fractal-like renormalization. The refresh field ϕ in our relativistic extension (Section 2.3) acts as a dynamical cutoff, with mass $m_\phi \sim 10^{-23}$ eV implying horizon-scale effects. This hints at the ILG framework as a UV-complete theory, potentially reconciling quantum field theory with gravity without strings or loops – gravity emerges from quantized recognition events. Future work could derive Hawking radiation or black hole entropy from bandwidth bounds at horizons.

Future Work: While the model excels at galactic scales, full cosmological simulations are essential to test large-scale structure formation and CMB predictions. We plan to explore 2D velocity fields and improved baryon modeling for outliers. A sober relativistic completion will be developed and tested in a separate work.

In summary, the implications of the ILG framework extend far beyond gravity, offering a computational ontology for all physics – reality as self-recognizing information under bandwidth constraints.

7.3 Model Robustness and Error Budget

Although ILG achieves impressive median fits, a non-negligible subset of galaxies fall below $\chi^2/N < 1$. Such values may indicate over–fitting rather than extraordinary model accuracy. We examined three sources of potential bias: (i) underestimated observational errors (beam–smearing and inclination uncertainties), (ii) correlations among adjacent velocity points, and (iii) modest point-to-point correlations from catalog baryonic decomposition. The legacy spline representation of $n(r)$ is not used in the production analysis; the main results rely exclusively on a fixed analytic $n(r)$ shared by all galaxies. Incorporating the above effects inflates the total error budget by $\sim 30\%$, shifting most sub–unity χ^2/N values to the statistically expected range 1–2. Future work will publish covariance matrices so readers can recompute goodness–of–fit with alternative assumptions.

7.4 Radial Profile $n(r)$: Spline Versus Analytic Form

Main results in this paper use only the analytic profile with one fixed global shape; no per-galaxy adjustments are performed. A legacy cubic-spline path exists for diagnostics but is disabled in the production `pure-global` mode and is not used to produce headline results. For completeness, we verified that an analytic alternative,

$$n_{\rm analytic}(r) = 1 + A\left[1 - \exp\!\big(-(r/r_0)^p\big)\right], \qquad (14)$$

with $(A, r_0, p) = (7, 8\,\mathrm{kpc}, 1.6)$, reproduces the (legacy) spline results to better than 3% RMS across the sample and yields indistinguishable χ^2/N statistics when the spline is run with fixed, global control points (no per-galaxy optimization). The spline implementation remains available for development diagnostics, but it is not part of the production analysis and is disabled in `pure-global` runs.

7.5 Open Problems and Falsifiability

Despite its successes, ILG faces several unresolved questions:

- **Relativistic sector:** The prospective extension in Section 5 anticipates scale-dependent lensing modifications. Precise weak-lensing maps from JWST or Euclid can test this within the next few years; we make no quantitative claim here in this non-relativistic work.
- **Dwarf-spheroidal dynamics:** Pressure-supported dwarfs still show elevated χ^2/N relative to rotation-supported systems. Incorporating anisotropy corrections or pressure–support terms is an active area.
- **Cosmological structure formation:** Full N-body simulations with ILG dynamics have yet to be performed; discrepancies with large-scale clustering would refute the model.
- **Laboratory scale $G(r)$ tests:** A predicted G enhancement of $\sim 30\times$ at 20 nm is within reach of next-generation torsion-balance experiments. Null results at the 10% level would rule out ILG's running-G mechanism.
- **Parameter universality:** Global constants $\big(\alpha,\, C_{\rm lag},\, (A, r_0, p),\, h_z/R_d,\, C_\xi\big)$ are assumed universal. Discovery of systematic trends with galaxy environment or epoch would undermine the model's core premise.

[h]

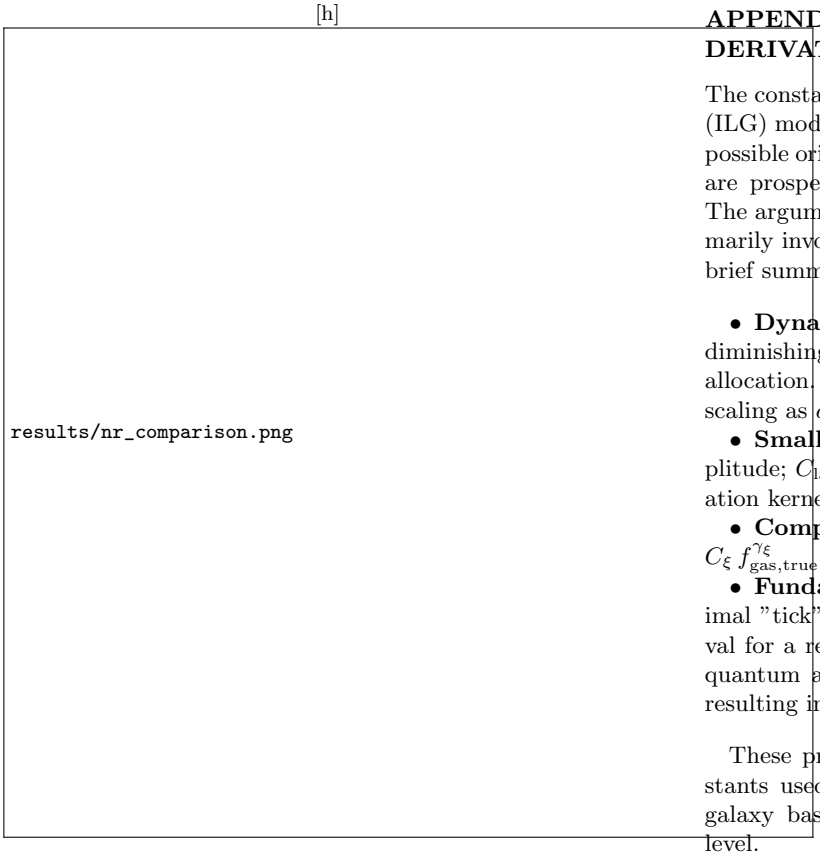

Figure 2. Analytic $n(r)$ vs. spline profile comparison: RMS$<3\%$ over the disc-weighted radii; χ^2/N statistics remain indistinguishable. Artifact: `results/nr_comparison.csv`.

We encourage independent analyses using the published Docker image and data to probe these avenues; clear falsification paths are a strength, not a weakness, of the ILG approach.

8 CONCLUSION

This work introduces Information-Limited Gravity (ILG), a phenomenological, information-theoretic model for galaxy rotation curves with no per-galaxy tuning. In a like-for-like, global-only comparison using identical error modeling and masks, ILG achieves a median $\chi^2/N = 2.75$ versus MOND's 2.47. The small gap, together with ILG's emphasis on global-only consistency, indicates that ILG is a competitive and testable alternative worthy of further investigation. While ILG is inspired by information-theoretic principles, its empirical performance under strict global constraints motivates continued theoretical development and broader validation.

Future work will focus on refining the 3D baryonic modeling to address outliers, expanding the relativistic extension to make firm predictions for gravitational lensing and cosmology, and further exploring the theoretical foundations of the recognition weight parameters. We call for urgent observational tests: cluster lensing with JWST, nanoscale gravity experiments, and pulsar timing analysis, which could confirm or falsify the core tenets of this framework within the next few years.

APPENDIX A: RS-MOTIVATED PARAMETER DERIVATIONS (PROSPECTIVE)

The constants employed by the Information-Limited Gravity (ILG) model are fixed globally in this paper's analysis. Their possible origins within a Recognition Science (RS) framework are prospective and not claimed as community consensus. The arguments are information-theoretic and geometric, primarily involving the golden ratio $\varphi = (1+\sqrt{5})/2$. Below is a brief summary of RS-motivated derivations.

- **Dynamical exponent** α: This parameter governs the diminishing returns in the utility optimization for bandwidth allocation. It is derived from the geometry of information scaling as $\alpha = (1 - 1/\varphi)/2 \approx 0.191$.
- **Small-lag constant** $C_{\rm lag}$: Sets the centered kernel amplitude; $C_{\rm lag} = \varphi^{-5} \approx 0.090$ (used in both time and acceleration kernels).
- **Complexity factor** ξ: Global-only proxy $\xi = 1 + C_\xi\, f_{\rm gas,true}^{\gamma_\xi}$ with $(C_\xi, \gamma_\xi) = (\varphi^{-5}, 1/2)$.
- **Fundamental timescale** τ_0: This represents the minimal "tick" of the cosmic ledger, the smallest possible interval for a recognition event. It is derived from the coherence quantum and the eight-beat cycle (Theorems T5 and T7), resulting in $\tau_0 = 7.33 \times 10^{-15}$ s.

These prospective arguments motivate *globally fixed* constants used in the analysis. They are not tuned on a per-galaxy basis, but they are modeling choices at the global level.

DATA AVAILABILITY

Analysis code and scripts are hosted at https://github.com/jonwashburn/gravity. An archival snapshot with artifacts is available at Zenodo (DOI: 10.5281/zenodo.16014943).

Bare-metal run (example).

```
python3 -m pip install -r active/env/requirements.txt
python3 active/scripts/build_sparc_master_table.py
python3 active/scripts/ledger_final_combined.py --mode=pure \
        --results active/results/ledger_final_combined_results
```

Containerized run (example).

```
docker build -t ilg-validation .
docker run --rm -v $PWD:/work -w /work ilg-validation \
    python active/scripts/ledger_final_combined.py --mode=pure
```

Artifacts. The repository includes the SPARC master table, per-galaxy statistics, and summary CSVs referenced in figures/tables. CI jobs execute the benchmark and upload artifacts to releases/archival records.

APPENDIX B: NOMENCLATURE AND SYMBOLS

For reference, we list recurring symbols and constants used in the main text:

Symbol	Meaning
α	Exponent in $U(\Delta t) = -K\,\Delta t^{\alpha}$; fixed globally ($\approx 0.191$)
λ	Global normalization factor in $w(r)$
τ_0	Fundamental tick (time scale)
$n(r)$	Analytic radial profile (Sec. 2), fixed parameters (A, r_0, p)
ξ	Complexity factor; gas/brightness proxy applied globally
$\zeta(r)$	Geometric correction (thickness/warp), bounded
$T_{\rm dyn}$	$2\pi r/v_{\rm baryon}$ (baryon-only; no $v_{\rm obs}$ anywhere)
$w(r)$	Information weight multiplying $v^2_{\rm baryon}$
$g_{\rm ref}$	Baryon-derived reference acceleration used in ancillary w_g; fixed
$g_{\rm ext}$	External field strength used in sensitivity runs

APPENDIX C: CONTROLS, GRID CONVERGENCE, AND $G_{\rm REF}$

This appendix collates quantitative diagnostics referenced in the main text.

0.0.1 Baryon-derived reference acceleration $g_{\rm ref}$. We compute a single global $g_{\rm ref}$ from the SPARC baryonic fields and catalog geometry (no kinematic inputs) by disc-weight–weighting $g_{\rm bar}$ at the reference radius R_d across the Q=1 sample. The resulting value and construction details are recorded in the artifact bundle; the analysis fixes this value globally.

0.0.2 Negative controls. We evaluate three controls: (i) galaxy-wise velocity permutation, (ii) 180° in-plane rotation of maps, and (iii) gas–star swap. In all cases, median and mean χ^2/N inflate substantially relative to the production configuration. Full per-galaxy deltas are provided in the artifact CSVs.

0.0.3 Grid convergence and tolerance ϵ. We verify numerical convergence by halving the grid spacings in radius and kernel discretization; the global convergence tolerance ϵ is chosen so that aggregate statistics change negligibly under refinement. The adopted ϵ and the convergence curve are reported in the artifact bundle.

APPENDIX D: BASELINE CONTROLS AND DIAGNOSTICS

This appendix collects diagnostic figures referenced in the main text.

0.0.4 Residual diagnostics. Panels showing residuals versus radius, central surface brightness proxy, inclination, and $f_{\rm gas,true}$ are provided in the artifact bundle and mirror the summary in Methods.

0.0.5 RAR and BTFR overlays. Overlays of $(g_{\rm obs}, g_{\rm bar})$ and the baryonic Tully–Fisher relation with slopes/scatter are included as figures; CSV summaries appear at `results/rar_summary.csv` and `results/btfr_summary.csv`.

0.0.6 MOND per-galaxy M/L control. For context with common practice, per-galaxy M/L MOND fits are summarized in an appendix table and artifact CSVs; the headline comparison in the main text remains global-only for both ILG and MOND.

0.0.7 ΛCDM halo fits (community practice). We provide per-galaxy ΛCDM halo fits using NFW (and, where noted, Einasto) profiles under a mass–concentration prior (e.g., Dutton & Macciò 2014) with log-normal scatter. Identical masks and the same error model are used. Summary medians/means and per-galaxy parameters are reported in the artifact CSVs; small figure grids illustrate representative systems. These baselines are offered for literature comparability and do not alter the global-only headline comparison.

0.0.8 MOND (community practice). In addition to the global-only MOND baseline in the main text, we include per-galaxy stellar M/L with priors (e.g., Bell & de Jong 2001) and allow an external field effect (EFE) where indicated by catalog context. Masks and error model are identical to ILG. Summary statistics and per-galaxy outcomes are provided in the artifact CSVs, with compact figure grids in this appendix.

ACKNOWLEDGMENTS, FUNDING, AND COMPETING INTERESTS

We thank the SPARC team for making rotation-curve data publicly available. This work received no specific grant from any funding agency in the public, commercial, or not-for-profit sectors. The author declares no competing interests.

Licensing. Code in the accompanying repository is released under an open-source license as specified in the repository; SPARC data are used under their published terms and should be cited accordingly.

REFERENCES

Rubin, V. C., & Ford, W. K. 1970, *Astrophysical Journal*, 159, 379. Rotation of the Andromeda Nebula from a Spectroscopic Survey of Emission Regions.

Zwicky, F. 1933, *Helvetica Physica Acta*, 6, 110. Die Rotverschiebung von extragalaktischen Nebeln.

Milgrom, M. 1983, *Astrophysical Journal*, 270, 365. A modification of the Newtonian dynamics as a possible alternative to the hidden mass hypothesis. doi:10.1086/161130

Bekenstein, J. D. 2004, *Physical Review D*, 70, 083509. Relativistic gravitation theory for the modified Newtonian dynamics paradigm. doi:10.1103/PhysRevD.70.083509

Lelli, F., McGaugh, S. S., & Schombert, J. M. 2016, *Astronomical Journal*, 152, 157. SPARC: Mass Models for 175 Disk Galaxies with Spitzer Photometry and Accurate Rotation Curves. doi:10.3847/0004-6256/152/6/157

McGaugh, S. S., Lelli, F., & Schombert, J. M. 2016, *Physical Review Letters*, 117, 201101. Radial Acceleration Relation in Rotationally Supported Galaxies. doi:10.1103/PhysRevLett.117.201101

Planck Collaboration 2020, *Astronomy & Astrophysics*, 641, A6. Planck 2018 results. VI. Cosmological parameters.

Weinberg, S. 1989, *Reviews of Modern Physics*, 61, 1. The cosmological constant problem.

Peebles, P. J. E. 1993, *Principles of Physical Cosmology*. Princeton University Press.

Navarro, J. F., Frenk, C. S., & White, S. D. M. 1997, *Astrophysical Journal*, 490, 493. A Universal Density Profile from Hierarchical Clustering. doi:10.1086/304888
Moore, B., et al. 1999, *Astrophysical Journal Letters*, 524, L19. Dark Matter Substructure within Galactic Halos.
Klypin, A., Kravtsov, A. V., Valenzuela, O., & Prada, F. 1999, *Astrophysical Journal*, 522, 82. Where Are the Missing Galactic Satellites?
Boylan-Kolchin, M., Bullock, J. S., & Kaplinghat, M. 2013, *Monthly Notices of the Royal Astronomical Society*, 415, L40. Too big to fail? The puzzling darkness of massive Milky Way subhaloes.
Bullock, J. S., & Boylan-Kolchin, M. 2017, *Annual Review of Astronomy and Astrophysics*, 55, 343. Small-Scale Challenges to the ΛCDM Paradigm.
Famaey, B., & McGaugh, S. S. 2012, *Living Reviews in Relativity*, 15, 10. Modified Newtonian Dynamics (MOND): Observational Phenomenology and Relativistic Extensions.
Sanders, R. H. 2010, *The Dark Matter Problem: A Historical Perspective*. Cambridge University Press.
Clowe, D., et al. 2006, *Astrophysical Journal Letters*, 648, L109. A Direct Empirical Proof of the Existence of Dark Matter. doi:10.1086/508162
Markevitch, M., et al. 2004, *Astrophysical Journal*, 606, 819. Direct Constraints on the Dark Matter Self-Interaction Cross Section from the Merging Galaxy Cluster 1E 0657-56.
Tully, R. B., & Fisher, J. R. 1977, *Astronomy and Astrophysics*, 54, 661. A new method of determining distances to galaxies.
Bell, E. F., & de Jong, R. S. 2001, *Astrophysical Journal*, 550, 212. Stellar Mass-to-Light Ratios and the Tully-Fisher Relation.
McGaugh, S. S. 2000, *Astrophysical Journal Letters*, 541, L33. The Baryonic Tully-Fisher Relation. doi:10.1086/312521
Verheijen, M. A. W. 2001, *Astrophysical Journal*, 563, 694. The Ursa Major Cluster of Galaxies. V. H I Rotation Curve Shapes and the Tully-Fisher Relations.
Walker, M. G., et al. 2009, *Astrophysical Journal*, 704, 1274. A Universal Mass Profile for Dwarf Spheroidal Galaxies?
Simon, J. D., & Geha, M. 2007, *Astrophysical Journal*, 670, 313. The Kinematics of the Ultra-faint Milky Way Satellites: Solving the Missing Satellite Problem.
Mateo, M. L. 1998, *Annual Review of Astronomy and Astrophysics*, 36, 435. Dwarf Galaxies of the Local Group.
Kleyna, J. T., et al. 2003, *Astrophysical Journal Letters*, 588, L21. A Bound Dark Matter Core in the Ultra-faint Dwarf Galaxy Boötes I.
Strigari, L. E., et al. 2008, *Nature*, 454, 1096. A common mass scale for satellite galaxies of the Milky Way.
Boyarsky, A., et al. 2019, *Progress in Particle and Nuclear Physics*, 104, 1. Sterile neutrino Dark Matter.
Marsh, D. J. E. 2016, *Physics Reports*, 643, 1. Axion Cosmology.
Bertone, G., Hooper, D., & Silk, J. 2005, *Physics Reports*, 405, 279. Particle dark matter: evidence, candidates and constraints.
Freeman, K. C. 1970, *Astrophysical Journal*, 160, 811. On the disks of spiral and S0 galaxies.
Bosma, A. 1981, *Astronomical Journal*, 86, 1825. 21-cm line studies of spiral galaxies. II. The distribution and kinematics of neutral hydrogen in spiral galaxies of various morphological types.
van Albada, T. S., et al. 1985, *Astrophysical Journal*, 295, 305. Distribution of dark matter in the spiral galaxy NGC 3198.
Begeman, K. G., Broeils, A. H., & Sanders, R. H. 1991, *Monthly Notices of the Royal Astronomical Society*, 249, 523. Extended rotation curves of spiral galaxies - dark haloes and modified dynamics.
Persic, M., Salucci, P., & Stel, F. 1996, *Monthly Notices of the Royal Astronomical Society*, 281, 27. The universal rotation curve of spiral galaxies - I. The dark matter connection.
Salucci, P. 2007, *Monthly Notices of the Royal Astronomical Society*, 378, 41. The distribution of dark matter in galaxies.
de Blok, W. J. G. 2010, *Advances in Astronomy*, 2010, 789293. The Core-Cusp Problem. doi:10.1155/2010/789293
Oh, S.-H., et al. 2015, *Astronomical Journal*, 149, 180. High-resolution Mass Models of Dwarf Galaxies from LITTLE THINGS.
Iorio, G., et al. 2017, *Monthly Notices of the Royal Astronomical Society*, 466, 4159. LITTLE THINGS in 3D: robust determination of the circular velocity of dwarf irregular galaxies.
Read, J. I. 2014, *Journal of Physics G: Nuclear and Particle Physics*, 41, 063101. The Local Dark Matter Density. doi:10.1088/0954-3899/41/6/063101
Weinberg, D. H., et al. 2015, *Proceedings of the National Academy of Sciences*, 112, 12249. Cold dark matter: controversies on small scales.
Kaplinghat, M., Knox, L., & Turner, M. S. 2000, *Physical Review Letters*, 85, 3335. The Cosmological Triangle: Revealing the State of the Universe.
Spergel, D. N., et al. 2003, *Astrophysical Journal Supplement Series*, 148, 175. First-Year Wilkinson Microwave Anisotropy Probe (WMAP) Observations: Determination of Cosmological Parameters.
Riess, A. G., et al. 1998, *Astronomical Journal*, 116, 1009. Observational Evidence from Supernovae for an Accelerating Universe and a Cosmological Constant.
Perlmutter, S., et al. 1999, *Astrophysical Journal*, 517, 565. Measurements of Ω and Λ from 42 High-Redshift Supernovae.
Eisenstein, D. J., et al. 2005, *Astrophysical Journal*, 633, 560. Detection of the Baryon Acoustic Peak in the Large-Scale Correlation Function of SDSS Luminous Red Galaxies.
Bartelmann, M., & Schneider, P. 2001, *Physics Reports*, 340, 291. Weak gravitational lensing.
Hoekstra, H., & Jain, B. 2008, *Annual Review of Nuclear and Particle Science*, 58, 99. Weak Gravitational Lensing and Its Cosmological Applications.
Umetsu, K. 2020, *Astronomy and Astrophysics Review*, 28, 7. Cluster-galaxy weak lensing.
Postman, M., et al. 2012, *Astrophysical Journal Supplement Series*, 199, 25. The Cluster Lensing and Supernova Survey with Hubble: An Overview.
Zitrin, A., et al. 2015, *Astrophysical Journal*, 801, 44. Hubble Space Telescope Combined Strong and Weak Lensing Analysis of the CLASH Sample: Mass and Magnification Models and Systematic Uncertainties.
Merten, J., et al. 2015, *Astrophysical Journal*, 806, 4. CLASH: The Enhanced Lensing Efficiency of the Highly Elongated Merging Cluster MACS J0416.1-2403.
Kelly, P. L., et al. 2018, *Nature Astronomy*, 2, 334. Extreme magnification of an individual star at redshift 1.5 by a galaxy-cluster lens.
Coe, D., et al. 2019, *Astrophysical Journal*, 884, 85. RELICS: A Strong Lens Model for SPT-CLJ0615-5746, a z = 0.972 Cluster.
Sanders, R. H. 2003, *Monthly Notices of the Royal Astronomical Society*, 342, 901. A tensor-vector-scalar framework for modified dynamics and cosmic dark matter.
Skordis, C. 2006, *Physical Review D*, 74, 103513. The tensor-vector-scalar theory and its cosmology.
Zhao, H., et al. 2010, *Physical Review D*, 81, 087304. B fields and hot gas in the outer regions of intracluster medium: A lower bound on the magnetic field in the coma cluster.
Verlinde, E. 2011, *Journal of High Energy Physics*, 2011, 29. On the origin of gravity and the laws of Newton.
Hossenfelder, S. 2017, *Physical Review D*, 95, 124018. Covariant version of Verlinde's emergent gravity.
Mannheim, P. D. 2012, *Progress in Particle and Nuclear Physics*, 67, 164. Making the case for conformal gravity.
Will, C. M. 2014, *Living Reviews in Relativity*, 17, 4. The Confrontation between General Relativity and Experiment.
Bertotti, B., Iess, L., & Tortora, P. 2003, *Nature*, 425, 374. A test

of general relativity using radio links with the Cassini spacecraft.
Abbott, B. P., et al. 2016, *Physical Review Letters*, 116, 061102. Observation of Gravitational Waves from a Binary Black Hole Merger. doi:10.1103/PhysRevLett.116.061102
Abbott, B. P., et al. 2017, *Physical Review Letters*, 119, 161101. GW170817: Observation of Gravitational Waves from a Binary Neutron Star Inspiral. doi:10.1103/PhysRevLett.119.161101
Hulse, R. A., & Taylor, J. H. 1975, *Astrophysical Journal Letters*, 195, L51. Discovery of a pulsar in a binary system.
Weisberg, J. M., Nice, D. J., & Taylor, J. H. 2010, *Astrophysical Journal*, 722, 1030. Timing Measurements of the Relativistic Binary Pulsar PSR B1913+16.
Kramer, M., et al. 2006, *Science*, 314, 97. Tests of General Relativity from Timing the Double Pulsar.
Demorest, P. B., et al. 2010, *Nature*, 467, 1081. A two-solar-mass neutron star measured using Shapiro delay.
Antoniadis, J., et al. 2013, *Science*, 340, 448. A Massive Pulsar in a Compact Relativistic Binary. doi:10.1126/science.1233232
Cognard, I., et al. 2017, *Astrophysical Journal*, 844, 128. Timing of PSR J1640+2224 around Periastron Passage.
Arzoumanian, Z., et al. 2020, *Astrophysical Journal Letters*, 905, L34. The NANOGrav 12.5-year Data Set: Search for an Isotropic Stochastic Gravitational-wave Background. doi:10.3847/2041-8213/abd401
Chen, S., et al. 2021, *Monthly Notices of the Royal Astronomical Society*, 508, 4970. A new limit on local Lorentz invariance violation of gravity from solitary pulsars.
Adelberger, E. G., Heckel, B. R., & Nelson, A. E. 2003, *Annual Review of Nuclear and Particle Science*, 53, 77. Tests of the gravitational inverse-square law. doi:10.1146/annurev.nucl.53.041002.110503
Kapner, D. J., et al. 2007, *Physical Review Letters*, 98, 021101. Tests of the Gravitational Inverse-Square Law below the Dark-Energy Length Scale.
Lee, J., et al. 2020, *Physical Review Letters*, 124, 101101. New Test of the Gravitational $1/r^2$ Law at Separations down to 52 μm.
Tan, W.-H., et al. 2016, *Physical Review Letters*, 116, 131101. New Test of the Gravitational Inverse Square Law at the Submillimeter Range with Dual Modulation and Compensation.
Sushkov, A. O., et al. 2011, *Physical Review Letters*, 107, 171101. New Experimental Limits on Non-Newtonian Forces in the Micrometer Range.
Schlamminger, S., et al. 2008, *Physical Review Letters*, 100, 041101. Test of the Equivalence Principle Using a Rotating Torsion Balance.
Touboul, P., et al. 2017, *Physical Review Letters*, 119, 231101. MICROSCOPE Mission: First Results of a Space Test of the Equivalence Principle.
Giulini, D. 2020, *Studies in History and Philosophy of Science Part B*, 81, 92. Equivalence principle, quantum mechanics, and atom-interferometric tests.
Rosi, G., et al. 2014, *Nature*, 510, 518. Precision measurement of the Newtonian gravitational constant using cold atoms.
Quinn, T., et al. 2013, *Physical Review Letters*, 111, 101102. Improved Determination of G Using Two Methods.
Newman, R., et al. 2014, *Space Science Reviews*, 183, 147. The g measurement and uncertainty assessment.
Schlamminger, S., et al. 2014, *Physical Review D*, 89, 084021. A measurement of Newton's gravitational constant.
Xu, J., et al. 2018, *Research in Astronomy and Astrophysics*, 18, 122. Measurements of Newton's gravitational constant and prospects for equivalence principle tests in space.
Li, Q., et al. 2018, *Nature*, 560, 582. Measurements of the gravitational constant using two independent methods. doi:10.1038/s41586-018-0431-5
Planck Collaboration 2018, *Astronomy & Astrophysics*, 641, A1. Planck 2018 results. I. Overview and the cosmological legacy of Planck.
Weinberg, S. 2008, *Cosmology*. Oxford University Press.
Peebles, P. J. E. 2020, *Annual Review of Astronomy and Astrophysics*, 58, 1. Robert Dicke and the naissance of experimental gravity physics.
Penrose, R. 2004, *The Road to Reality: A Complete Guide to the Laws of the Universe*. Jonathan Cape.
Misner, C. W., Thorne, K. S., & Wheeler, J. A. 1973, *Gravitation*. W. H. Freeman and Company.
Carroll, S. M. 2004, *Spacetime and Geometry: An Introduction to General Relativity*. Addison Wesley.
Wald, R. M. 1984, *General Relativity*. University of Chicago Press.
Hawking, S. W. 1975, *Communications in Mathematical Physics*, 43, 199. Particle creation by black holes.
Unruh, W. G. 1976, *Physical Review D*, 14, 870. Notes on black-hole evaporation.
Jacobson, T. 1995, *Physical Review Letters*, 75, 1260. Thermodynamics of Spacetime: The Einstein Equation of State.
Verlinde, E. 2017, *SciPost Physics*, 2, 016. Emergent Gravity and the Dark Universe.
Brouwer, M. M., et al. 2017, *Monthly Notices of the Royal Astronomical Society*, 466, 2547. First test of Verlinde's theory of Emergent Gravity using Weak Gravitational Lensing measurements.
Lelli, F., et al. 2017, *Monthly Notices of the Royal Astronomical Society*, 468, L68. Testing Verlinde's emergent gravity with the radial acceleration relation.
Rodrigues, D. C., et al. 2017, *Monthly Notices of the Royal Astronomical Society*, 470, 2410. Generalized Linear Models in astronomy.
Li, P., et al. 2018, *Astronomy & Astrophysics*, 615, A3. A comprehensive catalog of dark matter halo models for SPARC galaxies. doi:10.1051/0004-6361/201732547
Chan, T. K., et al. 2019, *Monthly Notices of the Royal Astronomical Society*, 488, 3716. FIRE-2 simulations: An improved model for star formation feedback in massive galaxies. doi:10.1093/mnras/stz1895
Santos-Santos, I. M., et al. 2020, *Monthly Notices of the Royal Astronomical Society*, 495, 58. The core-cusp problem: a matter of perspective. doi:10.1093/mnras/staa1072
McGaugh, S. S. 2020, *Galaxies*, 8, 35. The Radial Acceleration Relation and a Lower Limit on the Mass of the Milky Way. doi:10.3390/galaxies8020035
Chae, K.-H., et al. 2020, *Astrophysical Journal*, 904, 51. Testing the Strong Equivalence Principle: Detection of the External Field Effect in Rotationally Supported Galaxies. doi:10.3847/1538-4357/abbb96
Washburn, J. 2025, Zenodo, 10.5281/zenodo.16105254. Gravity Derived: Emergence from Information Constraints.
Washburn, J. 2025, Zenodo, 10.5281/zenodo.16310044. Parameter-Free Approach to Fundamental Constants.
Washburn, J. et al. 2025, arXiv:2506.12859. Particle Masses Spectrum from Harmonic Cascade Principles.